

Multi-component states for trapped spin-1 Bose-Einstein Condensates in the presence of magnetic field

Projjwal K. Kanjilal^{1,*} and A. Bhattacharyay^{1,†}

¹*Department of Physics, Indian Institute of Science Education and Research, Dr. Homi Bhabha Road, Pune 411 008, India*
(Dated: January 18, 2023)

In presence of a magnetic field, the multi-component ground states appear for trapped spin-1 Bose-Einstein condensates for both ferromagnetic and anti-ferromagnetic types of spin-spin interaction. We aim to produce an accurate analytical description of the multi-components states which is of fundamental importance. First, we show the analytical results provided by the Thomas-Fermi approximation, which is one of the most trusted and widely used analytical method. Despite being in the regime of Thomas-Fermi approximation, it provides wrong physical conclusions. We generalize the variational method introduced in the article [1] and demonstrate that the variational method is crucial in giving a proper analytical description of the multi-component states which is also backed by numerical simulation.

I. INTRODUCTION

The successful experimental realization of Bose-Einstein condensates (BEC) with alkali atoms [2–4] inside a magnetic trap spurred renewed interest [5–7] in ultracold atomic physics. Soon it attracted a lot of attention from both atomic- and condensed-matter physics communities as it provided an ideal test bed as a quantum simulator [8–13] and precision measurements [14–19] for its unprecedented experimental control.

The early experiments on BEC [20–22] were done in the magnetic trap which only captures atoms with weak-field-seeking hyperfine states, thus, the magnetic degrees of freedom were frozen in the resulting BEC. Later, with the optical trapping technique this limitation was overcome, and spinor BECs were created with all the hyperfine states of the constituent spin- f atoms (f is an integer) [23–25]. The order parameter of such a system constitutes $(2f + 1)$ components. Due to the interplay of magnetic field and interatomic interaction, the spinor BEC shows a rich variety of phenomena including spin-textures [26, 27], domain structures [28–47], and topological phases [48]. Spinor BEC also attracted a lot of attention due to its complex soliton structures [49–52], interesting few-body physics in low dimensions [53].

The role of the multi-component ground state where more than one spin-projections is populated is crucial for the plethora of interesting phenomena that occurs in spinor BEC. As a result, there has been a lot of seminal studies on multi-component ground states [54–57]. But most of the analytical studies focus on the single-mode approximation which is only followed in absence of a magnetic field. In this article, we look at the ground state structures involving the multi-modal multi-component stationary states of confined spin-1 BEC in the presence of the magnetic field without any finite temperature [58–60] or inter-particle correlation effects [61]. The contri-

bution of the magnetic field comes into play in terms of linear and quadratic Zeeman terms (p, q respectively) that are present in the Gross-Pitaevskii (GP) equation which governs the dynamics of the three component order parameter (the mean fields ψ_1, ψ_0 and ψ_{-1}). In absence of trapping, solving the GP equation one can get to the phase diagram in p, q parameter space [25, 62, 63]. In a realistic situation, the potential energy due to trapping and interaction along with the kinetic energy play important role in determining the ground state properties. To get an analytical description for such a situation one takes resorts to the Thomas-Fermi (T-F) approximation which is a well-known method for its simplicity and accuracy at large particle number limit. It is well-accepted that the T-F approximation produces ground state structures with reasonable accuracy if the density is high enough to neglect the kinetic energy term in comparison to interaction terms. However, there exist reasons for the breakdown of T-F approximation for competing ground state candidates of comparable free energy even for large condensates as well as small ones.

In this article, we present such a situation where the kinetic term is actually negligible in comparison to the interaction terms and hence in the range of applicability of the T-F approximation. But, the T-F provides the wrong physical conclusion. Such a situation arises in a multi-modal multi-component ground state where the density of the sub-components varies quite a lot. T-F approximation in such cases wrongly predicts a domain formation of multi-component states along with a peripheral single-component state. However, a detailed investigation beyond T-F approximation would reveal the actual scenario which is shown in this paper. We have extended and generalized the formalism of the multi-modal variational method, introduced in the article [1] for a simplistic situation in absence of the magnetic field. We will show that this generalized formalism provides quite an accurate description in comparison with the numerically obtained number density profiles.

One of the key findings of this article is that the T-F approximation requires significant correction for multi-

* projjwal.kanjilal@students.iiserpune.ac.in

† a.bhattacharyay@iiserpune.ac.in

component stationary states that also become the ground state for spin-1 BEC under trapping. It also comes out from the present analysis that one cannot avoid a multi-modal analysis while dealing with such multi-component ground states to correct for limitations of T-F approximation. We consider quasi-one-dimensional ^{87}Rb and ^{23}Na systems under harmonic trapping. For the ^{87}Rb , T-F approximation predicts a domain-like structure between the phase-matched state near the center of the trap followed by the polar state outside. Similarly, for a specific choice of Zeeman terms, the T-F approximation predicts the ground state to be a domain structure between the anti-ferromagnetic and ferromagnetic states. Using the generalized multi-modal variational method, we show that there is no domain structure in the ground states of the above-mentioned cases. The multi-component stationary states at the core of the trap are actually the ground states. The results of the variational method are validated through a comparison with the numerical simulation.

The article is organized as follows: In section II, we discuss the mean-field theory of the spin-1 trapped BEC in presence of the magnetic field. In section III we focus on the analytical description of the phase-matched state and the anti-ferromagnetic state that becomes the ground state for ^{87}Rb and ^{23}Na , respectively. We start with the T-F results and then we provide a description based on the variational method compare it with the numerical simulation. In this section, we also discuss why T-F approximation cannot be trusted and the variational method must be used for multi-component states. This follows with a short discussion about the generality of the treatment presented here and possible directions to explore.

II. MEAN FIELD THEORY: GP EQUATION

The dynamics of the mean fields for a trapped spin-1 BEC in presence of the magnetic field is captured in the Gross-Pitaevskii (GP) equation [47, 54, 63, 64],

$$i\hbar \frac{\partial \psi_m}{\partial t} = \left(-\frac{\hbar^2 \nabla^2}{2M} + U(\vec{r}) - pm + qm^2 + c_0 n \right) \psi_m + c_1 \sum_{m'=-1}^1 \vec{F} \cdot \vec{f}_{mm'} \psi_{m'}, \quad (1)$$

where the first term on the r.h.s of Eq.1 is the kinetic energy contribution for particles of mass M . The second term is due to the confining potential and the presence of the magnetic field is captured by the linear and quadratic Zeeman terms p and q respectively. We assume a two-body contact interaction that can be decomposed into spin-independent (the term involving c_0) and inter-spin interactions (the term with c_1). As this is a spin-1 sys-

tem, the suffix m and m' take the values 1, 0 and, -1 .

The total density n is defined as,

$$n(r) = \sum_{m=-1}^1 |\psi_m|^2, \quad (2)$$

and the local spin density \vec{F} is

$$\vec{F} = \sum_{i,j=-1}^1 \psi_i^* \vec{f}_{ij} \psi_j, \quad (3)$$

where the \vec{f} is defined via the spin-1 Pauli matrices [63]. So, Eq.1 is the GP equation which is a set of three coupled non-linear partial differential equations which yields the order parameter $(\psi_1, \psi_0, \psi_{-1})$ as its solution.

The mean-field approximated total energy, [63]

$$E = \int d\vec{r} \sum_{m=-1}^1 \psi_m^* \left(-\frac{\hbar^2 \nabla^2}{2M} + U_{trap}(\vec{r}) - pm + qm^2 \right) \psi_m + \frac{c_0}{2} n^2 + \frac{c_1}{2} |\vec{F}|^2, \quad (4)$$

can be compared for different stationary states to get to the ground state of the system. In this paper, we represent the stationary states by notation (n_1, n_0, n_{-1}) , where, n_m is the placeholder for the binary notation, 0 or 1. If the sub-components are populated we represent it as 1 and if unpopulated we represent it as 0. In this notation, for example, the ferromagnetic state is represented as $(1, 0, 0)/(0, 0, 1)$ where the sub-component corresponding to $m = 1$ or $m = -1$ is populated.

To simplify the GP equations further, one can write the mean fields in terms of the density and corresponding phase,

$$\psi_m(\vec{r}, t) = \sqrt{n_m(\vec{r})} \exp(-\frac{i\mu t}{\hbar}) \exp(-i\theta_m), \quad (5)$$

where the parameter μ stands for chemical potential. One can get the number and phase dynamics separately [47] by using the ansatz Eq.5 in the GP equation Eq.1,

$$\dot{n}_0(\vec{r}) = -\frac{4c_1 n_0 \sqrt{n_1 n_{-1}} \sin \theta_r}{\hbar}, \quad (6)$$

$$\dot{n}_{\pm 1}(\vec{r}) = \frac{2c_1 n_0 \sqrt{n_1 n_{-1}} \sin \theta_r}{\hbar}, \quad (7)$$

$$\hbar \dot{\theta}_0 = \frac{1}{\sqrt{n_0(\vec{r})}} (\mathcal{H} - \mu) \sqrt{n_0(\vec{r})} + c_1 (n_1 + n_{-1} + 2\sqrt{n_{-1} n_1} \cos \theta_r), \quad (8)$$

$$\hbar\dot{\theta}_{\pm 1} = \frac{1}{\sqrt{n_{\pm 1}(\vec{r})}} (\mathcal{H} - \mu) \sqrt{n_{\pm 1}(\vec{r})} \pm c_1 (n_1 - n_{-1}) + q \mp p + c_1 n_0 \left(1 + \sqrt{\frac{n_{\mp 1}(\vec{r})}{n_{\pm 1}(\vec{r})}} \cos \theta_r \right), \quad (9)$$

where, $\mathcal{H} = -\frac{\hbar^2 \nabla^2}{2M} + U(\vec{r}) + c_0 n$. The relative phase θ_r in Eq.8-9 is defined as, $\theta_r = \theta_1 + \theta_{-1} - 2\theta_0$ [63]. The same ansatz Eq.5 makes the energy (Eq.4) a function of the sub-component number density and the relative phase,

$$\begin{aligned} E &= \int d\vec{r} e(\vec{r}) \\ &= \int d\vec{r} \left(- \sum_{m=-1}^1 \sqrt{n_m(\vec{r})} \frac{\hbar^2 \nabla^2}{2M} \sqrt{n_m(\vec{r})} \right. \\ &\quad + U(\vec{r}) n(\vec{r}) - p(n_1 - n_{-1}) + q(n_1 + n_{-1}) \quad (10) \\ &\quad + \frac{c_0}{2} n^2(\vec{r}) + \frac{c_1}{2} (n_1 - n_{-1})^2 \\ &\quad \left. + c_1 n_0 [n_1 + n_{-1} + 2\sqrt{n_1 n_{-1}} \cos \theta_r] \right), \end{aligned}$$

where $e(\vec{r})$ is the energy density. Note that we are not interested in vortex solutions, so in Eq.6-10 we have neglected spatial variation of the sub-component phases assuming phases to be either constant or varying slowly.

For the stationary states, there is no temporal variation of the sub-component number density and the sub-component phases i.e., the l.h.s of the Eq.6-9 can be equated to zero. From the number density variation equations (Eq.6-7), one can conclude that at least one of the sub-components should be empty to satisfy the equations. Otherwise, if all the sub-components are populated, then the relative phase can either be 0 or π . When all the sub-components are populated, the stationary state where $\theta_r = 0$ is satisfied is also known as the phase-matched (PM) state whereas for $\theta_r = \pi$ one gets the anti-phase-matched (APM) state. The sub-component phase equations (Eq.8-9) for a particular stationary state can be solved to get the sub-component number densities. Before going into that, let us get these equations in a non-dimensional form.

The system considered is in quasi-one-dimensional harmonic confinement, i.e., the condensate is elongated along the x-axis. This means the trapping frequency along the x-direction is much less than the geometric mean of the trapping frequency along the other two directions i.e., $\omega_x \ll \sqrt{\omega_{xy}}$, where $\omega_{yz} = \sqrt{\omega_y \omega_z}$. One can scale the number density and the interaction parameters as [1],

$$c_0 = 2\pi l_{yz}^2 l_x \lambda_0^{1D} \hbar \omega_x, \quad c_1 = 2\pi l_{yz}^2 l_x \lambda_1^{1D} \hbar \omega_x, \quad (11)$$

$$u_m = 2\pi l_{yz}^2 l_x n_m, \quad r = l_x \zeta \quad (12)$$

where, $l_x^2 = \hbar/(m\omega_x)$, $l_{yz}^2 = \hbar/(m\omega_{yz})$, and N is the total number of particles in the condensate. As a result, the parameters λ_0^{1D} , λ_1^{1D} , ζ and u_m become all dimensionless.

Three phase-stationary equations Eq.8-9 can now be written as,

$$\left\{ -\frac{1}{2} \frac{d^2}{d\zeta^2} + \frac{1}{2} \zeta^2 + \lambda_0 u - \mu' \right. \quad (13)$$

$$\left. + \lambda_1 (u_1 + u_{-1} + 2\sqrt{u_{-1} u_1} \cos \theta_r) \right\} \sqrt{u_0} = 0,$$

$$\left\{ -\frac{1}{2} \frac{d^2}{d\zeta^2} + \frac{1}{2} \zeta^2 + \lambda_0 u - \mu' \pm \lambda_1 (u_1 - u_{-1}) \right. \quad (14)$$

$$\left. \pm p' + q' \right\} \sqrt{u_{\pm 1}} + \lambda_1 u_0 (\sqrt{u_{\pm 1}} + \sqrt{u_{\mp 1}} \cos \theta_r) = 0.$$

where, μ' , p' , and q' are the scaled parameters for chemical potential, the linear and quadratic Zeeman terms respectively. The scaling is done by dividing these parameters with the factor $(\hbar \omega_x)$. The sub-component densities add up to provide the total density of the system, i.e. $u = u_1 + u_0 + u_{-1}$.

If the kinetic term is negligible in comparison to interaction terms, then one can use the T-F approximation and solve these three equations to get the sub-component number densities for the stationary state. Thus, by substituting the sub-component densities in Eq.10 one can get the energy or the energy density of the stationary states. The T-F predicted ground states of our present interest are detailed in Table 1.

III. MULTI-COMPONENT STATIONARY STATES:

Consider a quasi-one dimensional cigar-shaped harmonic confinement of trapping frequency along the elongated direction $\omega_x = 2\pi \times 50 \text{ Hz}$ and the geometric mean of the trapping frequencies along the transverse direction $\omega_{yz} = 2\pi \times 1261 \text{ Hz}$. In the article [1], it was shown that for 1-D trapping geometry with the same trapping frequency, the T-F approximation gives reasonably good results in predicting the sub-component densities for single component stationary states for $N \geq 500$ in the absence of magnetic field. There is reason to believe that T-F approximation might produce fairly accurate results for multi-component stationary states in presence of a small magnetic field if $N \geq 500$. For the case studies in this paper, the number of condensate particles is fixed at $N = 5000$ for which T-F should produce even bet-

States	Variation of density	Energy density	Restriction
(1,0,0) F1	$(\lambda_0 + \lambda_1)u(\zeta) = \mu' + p' - q' - \zeta^2/2$	$\frac{[\zeta^2/2 - p' + q'][\mu' + p' - q' - \zeta^2/2]}{(\lambda_0 + \lambda_1)} + \frac{[\mu' + p' - q' - \zeta^2/2]^2}{2(\lambda_0 + \lambda_1)}$	none
(0,1,0) P	$\lambda_0 u(\zeta) = \mu' - \zeta^2/2$	$\frac{\zeta^2/2[\mu' - \zeta^2/2]}{\lambda_0} + \frac{[\mu' - \zeta^2/2]^2}{2\lambda_0}$	none
(0,0,1) F2	$(\lambda_0 + \lambda_1)u(\zeta) = \mu' - p' - q' - \zeta^2/2$	$\frac{[\zeta^2/2 + p' + q'][\mu' - p' - q' - \zeta^2/2]}{(\lambda_0 + \lambda_1)} + \frac{[\mu' - p' - q' - \zeta^2/2]^2}{2(\lambda_0 + \lambda_1)}$	none
(1,0,1) AF	$\lambda_0 u(\zeta) = \mu' - q' - \zeta^2/2$ and $(u_1 - u_{-1}) \equiv F_z = \frac{p'}{\lambda_1}$	$\frac{[\zeta^2/2 + q'][\mu' - q' - \zeta^2/2]}{\lambda_0} + \frac{[\mu' - q' - \zeta^2/2]^2}{2\lambda_0} - \frac{p'^2}{2\lambda_1}$	none
(1,1,1) (A)PM	$(\lambda_0 + \lambda_1)u(\zeta) = k_1 - \zeta^2/2$ where, $k_1 = \mu' + \frac{(p'^2 - q'^2)}{2q'}$	$\frac{\zeta^2/2[k_1 - \zeta^2/2]}{\lambda_0 + \lambda_1} + \frac{\lambda_1}{2} \left[\frac{k_1 - \zeta^2/2}{\lambda_0 + \lambda_1} - \frac{p'^2 - q'^2}{2q'\lambda_1} \right]^2 + \frac{\lambda_0}{2} \left[\frac{k_1 - \zeta^2/2}{\lambda_0 + \lambda_1} \right]^2$	PM ($ p' < q' $) APM ($ p' > q' $)

Table I. The density and the energy density expressions corresponding to different stationary states at $\lambda_1 \neq 0$ obtained via T-F approximation are shown here [47]. All the parameters in this table are in dimensionless form. One can use Eq. 11-12 to convert expressions into dimensional forms. The energy expressions and the density expressions for PM and APM states are identical. However, PM and APM states are restricted in space where APM state exists if the absolute value of the linear Zeeman term is higher than that of the quadratic Zeeman term and PM state exists otherwise.

ter results. However, in what follows we will show that even at such a high particle number T-F results falter and corrections are needed.

Our present focus is on the PM state which is a multi-component state that appears as a ground state for a range of p and q values in condensates with the ferromagnetic spin-spin interaction e.g., ^{87}Rb . The anti-ferromagnetic state that becomes the ground state for ^{23}Na where the spin-spin interaction is of anti-ferromagnetic type [63] is also discussed in this paper. Note that, the quasi-one-dimensional confinement is taken for convenience in numerical simulation. However, the analytic formalism developed and validated is general and can be extended to higher dimensional cases where numerical analysis could be problematic. In the following, we show the results of the T-F study for these two cases, in order to be able to draw a detailed comparison with the beyond T-F results later.

A. PM state: T-F study

For ^{87}Rb condensate with ferromagnetic type interaction, the numerical values of the parameters corresponding to the trap geometry are $l_x = 1.53 \mu\text{m}$, $l_{yz} = 0.30 \mu\text{m}$, $\lambda_0 = 17.66 \times 10^{-3}$ and $\lambda_1 = -6.22 \times 10^{-4}$. In this section, to compare the T-F result with the numerical profile as a case study the linear and quadratic Zeeman terms are fixed at $p' = 0.01$ and $q' = 0.3$. The stationary state that is energetically favorable to be ground state at these parameter values is the PM state. Note that, the conclusions, however, are not dependent on a specific choice of parameter values but rather will remain valid for a range of p' and q' values for which the PM state is favorable as the ground state.

The sub-component number densities of the PM state

are [47],

$$u_1^{TF} = \frac{(p' + q')^2}{4q'^2} \left[\frac{\mu' + \frac{(p'^2 - q'^2)}{2q'} - \frac{1}{2}\zeta^2}{\lambda_0 + \lambda_1} + \frac{q'^2 - p'^2}{2\lambda_1 q'} \right], \quad (15)$$

$$u_{-1}^{TF} = \frac{(p' - q')^2}{4q'^2} \left[\frac{\mu' + \frac{(p'^2 - q'^2)}{2q'} - \frac{1}{2}\zeta^2}{\lambda_0 + \lambda_1} + \frac{q'^2 - p'^2}{2\lambda_1 q'} \right], \quad (16)$$

$$u_0^{TF} = \frac{(q'^2 - p'^2)}{2q'^2} \left[\frac{\mu' + \frac{(p'^2 - q'^2)}{2q'} - \frac{1}{2}\zeta^2}{\lambda_0 + \lambda_1} - \frac{q'^2 + p'^2}{2\lambda_1 q'} \right], \quad (17)$$

which can be compared with the numerically simulated profiles. For the purpose of numerical simulation, imaginary time propagation in the split-step Fourier method [65] is used. The number density profiles as predicted by the T-F are used as initial seeds.

Comparison of the sub-component densities of T-F profiles with the numerical ones reveals very good agreement for the sub-components u_1 and u_{-1} . The profile for the u_0 component also agrees in the high-density region of the trap Fig. 1(a), but starts to deviate when the other components u_1 and u_{-1} vanish which for this parameter values is at around $\zeta_{\pm 1}^{TF} = \pm 10.3$. Note that, $\zeta_{\pm 1}^{TF}$ is the T-F radius of the $u_{\pm 1}$ components. Naturally, one might expect that, beyond the point, $\zeta_{\pm 1}^{TF}$, the summation of the T-F approximated sub-component number densities

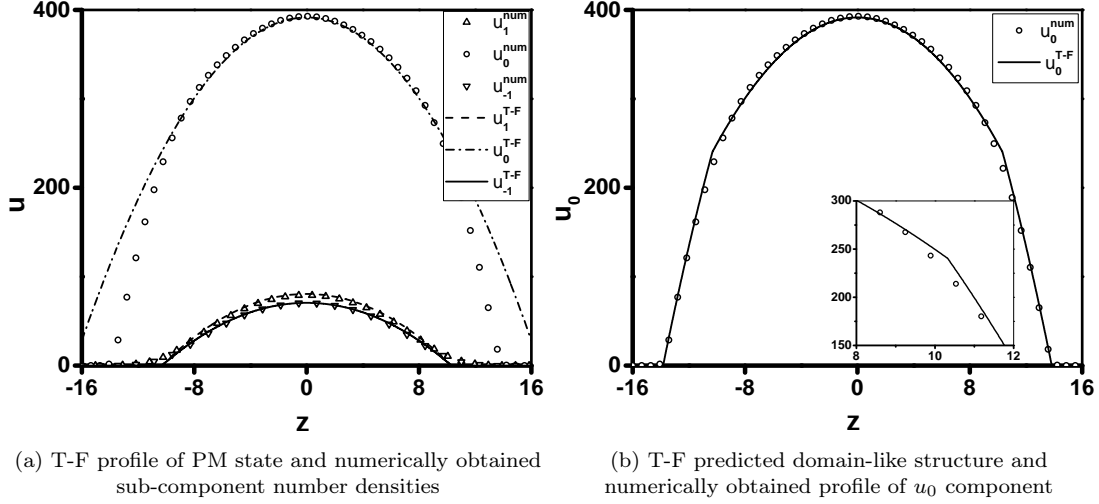


Figure 1. Subfig-(a): The T-F sub-component number densities for PM state is compared with the numerical densities for the parameter value $p' = 0.01$ and $q' = 0.3$. The T-F approximated u_0 expression corresponding to PM state (shown in dash-dot line) starts to disagree with that of the numerical simulation beyond $|\zeta| > 10.3$, which is the T-F radius of the $u_{\pm 1}$ component. Subfig-(b): The T-F prediction of the domain-like situation is plotted where, the u_0 component (solid line) follows the T-F expression of the PM state when all the sub-components are populated ($|\zeta| < 10.3$ for this case), followed by a polar state-like behavior. Note that discontinuity appears in the u_0 (inset) while the numerical result is smooth (bubble markers).

(i.e., $u_{tot} = u_1 + u_0 + u_{-1}$) will not agree with the numerical profile as there is a significant mismatch in the u_0 component.

This is quite natural as the PM state is only defined as long as all the sub-components are populated. However, PM state exists only until the u_1 and u_{-1} vanish (according to T-F calculations) at $\zeta = 10.3$. So, within the T-F picture, it can be said that near the center of the harmonic trap, the PM state is occupied but as the $u_{\pm 1}$ goes to zero, the PM state ceases to exist. For $|\zeta| > 10.3$, only the u_0 component is present, which signifies that it is the polar state that occupies the low-density region Fig.1(b).

The sub-component number densities for such a construct can be given as,

$$u_1^{TF} = \frac{(p' + q')^2}{4q'^2} \left[\frac{\mu' + \frac{(p'^2 - q'^2)}{2q'} - \frac{1}{2}\zeta^2}{\lambda_0 + \lambda_1} + \frac{q'^2 - p'^2}{2\lambda_1 q'} \right], \quad (18)$$

$$u_{-1}^{TF} = \frac{(p' - q')^2}{4q'^2} \left[\frac{\mu' + \frac{(p'^2 - q'^2)}{2q'} - \frac{1}{2}\zeta^2}{\lambda_0 + \lambda_1} + \frac{q'^2 - p'^2}{2\lambda_1 q'} \right], \quad (19)$$

$$u_0^{TF} = \begin{cases} \frac{(q'^2 - p'^2)}{2q'^2} \left[\frac{\mu' + \frac{(p'^2 - q'^2)}{2q'} - \frac{1}{2}\zeta^2}{\lambda_0 + \lambda_1} - \frac{q'^2 + p'^2}{2\lambda_1 q'} \right], & \text{if } |\zeta| \leq \zeta_{\pm 1}^{TF} \\ \frac{\mu'_{polar} - \frac{1}{2}\zeta^2}{\lambda_0}, & \text{otherwise,} \end{cases}$$

where, $\zeta_{\pm 1}^{TF}$ is the Thomas-Fermi radius of the $u_{\pm 1}$ component for this 1-D geometry.

As can be seen in Fig.1(b) this domain-like explanation works really well as we compare the sub-component density with the numerical u_0 , but there will be a discontinuity at $|\zeta| = \zeta_{\pm 1}^{TF}$. The slope of analytical u_0 also changes drastically around this point resulting in a lot of kinetic energy cost.

If we add the sub-component densities of the PM state given by expressions Eq.15-17 one arrives at the total number density,

$$u_{tot}^{PM} = \frac{\mu' + \frac{(p^2 - q^2)}{2q} - \frac{1}{2}\zeta^2}{\lambda_0 + \lambda_1}, \quad (20)$$

as long as all the sub-components are populated, a necessary condition for the validity of PM state. As the number density cannot be negative, at $|\zeta| > |\zeta_{\pm 1}^{TF}|$ where the $u_{\pm 1}^{TF}$ goes to zero, the above expression is not valid beyond the TF radius of the $u_{\pm 1}$ components. Also, the PM state does not exist beyond this point.

In Fig.2, we notice that the total number density obtained from the numerical simulation can be aptly de-

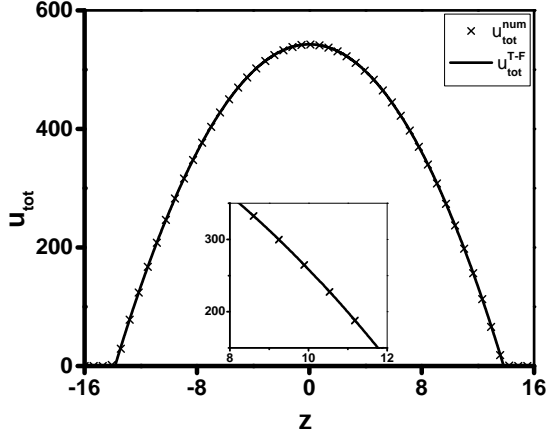


Figure 2. The total density obtained from numerical simulation matches quite well with the expression Eq.20, which is the T-F expression corresponding to the total density of the PM state. Surprisingly, this expression of total number density is only valid as long as all the sub-components are populated. (inset) The same expression matches with the numerical total density even beyond the T-F radius of the $u_{\pm 1}$ component which is roughly at $|\zeta| \simeq 10.3$.

scribed by the analytical expression Eq.20. The element of surprise is that even beyond $|\zeta_{\pm 1}^{TF}|$, where according to T-F the PM state ceases to exist, the numerical profile of total number density agrees with Eq.20.

The above conclusion about the discontinuity in the u_0 component and hence the limitations of T-F approximation can be further strengthened if we compare numerical simulation and T-F prediction for a different spin-spin interaction, $c_1 \rightarrow 5c_1^{Rb}$ while keeping all other parameter values the same. Experimentally, this is possible via Feshbach resonance [66].

For this choice of parameter values, the domain-like structure predicted by T-F has a more visible discontinuity (Fig.3(a)) for the sub-component u_0 at $|\zeta_{\pm 1}^{TF}| = 13.13$. The total density for this domain-like structure will also have that same discontinuity. Whereas, in Fig.3(b) we verify that the numerical density and the Eq.20 are in agreement near the T-F radius of $u_{\pm 1}$ and only deviates near the T-F radius of the u_0 component itself (inset of Fig.3(b)).

To explain this, one has to remember that T-F approximation tells that the $u_{\pm 1}$ sharply goes to zero at $|\zeta| = \zeta_{\pm 1}^{TF}$ but in reality that cannot be the case. We need to include the kinetic energy term in the analysis. As a result, near this point the Laplacian terms in Eq.14 cannot be neglected. However, one can ignore the Laplacian term in Eq.13 as the u_0 component is still in the high-density region near this point. As the phase dynamics GP equations are coupled, one has to solve the Eq.13-14 by keeping the Laplacian terms corresponding to $u_{\pm 1}$ components. This shows that the T-F approximation is bound to produce an inaccurate description of multi-component stationary states even in the so-called "T-F

regime". This warrants a need for an accurate analytical description of the multi-component states appearing for the spin-1 BEC.

B. PM state: The variational method

In the article [1], a multi-modal variational method was introduced which incorporates the kinetic contribution and produces the sub-component number-density profile of a stationary state with great accuracy. The variational method (VM) was developed for a spin-1 BEC in absence of a magnetic field which works really well even for condensates with a small number of particles where the T-F approximation was shown to be no longer valid. The PM state was also analyzed using the multi-modal VM, but for $p = 0$ and $q = 0$ the PM state sub-component densities are of the same spatial mode, therefore, reducing significant complexity.

We extend the same procedure here in presence of a magnetic field. The number densities of the PM state are multi-modal in spatial variation, thus, the situation is much more complex but the extended VM tackles it with ease. In this section we will briefly discuss the procedure; for a more elaborate description see appendix A.

For the variational method to work, we need to estimate the sub-component densities in the high-density region from the G-P equations Eq.13-14 by neglecting the kinetic energy contribution. This is followed by an assumption of the Gaussian-like tail in the low-density region. So the sub-component densities are defined as,

$$u_{\pm 1,0}^{in} = g_{\pm 1,0}(\mu', \zeta), \quad \text{for } |\zeta| \leq \zeta_{\pm 1,0}^{mat} \quad (21)$$

$$u_{\pm 1,0}^{out} = (a_{\pm 1,0} + c_{\pm 1,0}|\zeta| + d_{\pm 1,0}\zeta^2) \exp\left(-\frac{\zeta^2}{b_{\pm 1,0}}\right) \quad (22)$$

for $|\zeta| \geq \zeta_{\pm 1,0}^{mat}$;

where $g_{\pm 1,0}(\mu', \zeta)$ is the functional form of the sub-component density $u_{\pm 1,0}$ near the center of the trap. In the low-density region, we assume the number density (or the wave function) taking into account the first few oscillator states.

To determine the unknown coefficients a_m, b_m, c_m, d_m with $m = \pm 1, 0$, we impose a smooth matching condition at $|\zeta| = \zeta^{mat}$ where the $\sqrt{u_{\pm 1,0}}$ and their first three derivatives become equal for low- and high-density expressions. The third derivative matching ensures a smooth kinetic energy profile as well. From these four conditions, one can determine all four coefficients appearing in Eq.22, which now become functions of μ' and $\zeta_{\pm 1,0}^{mat}$. The parameter μ' can be expressed in terms of $\zeta_{\pm 1,0}^{mat}$ from the number conservation equation (see appendix A). Following this step, the densities (and as a result), the total energy can be written only as a function of the matching points $\zeta_{\pm 1,0}^{mat}$ which are the only variables left. These

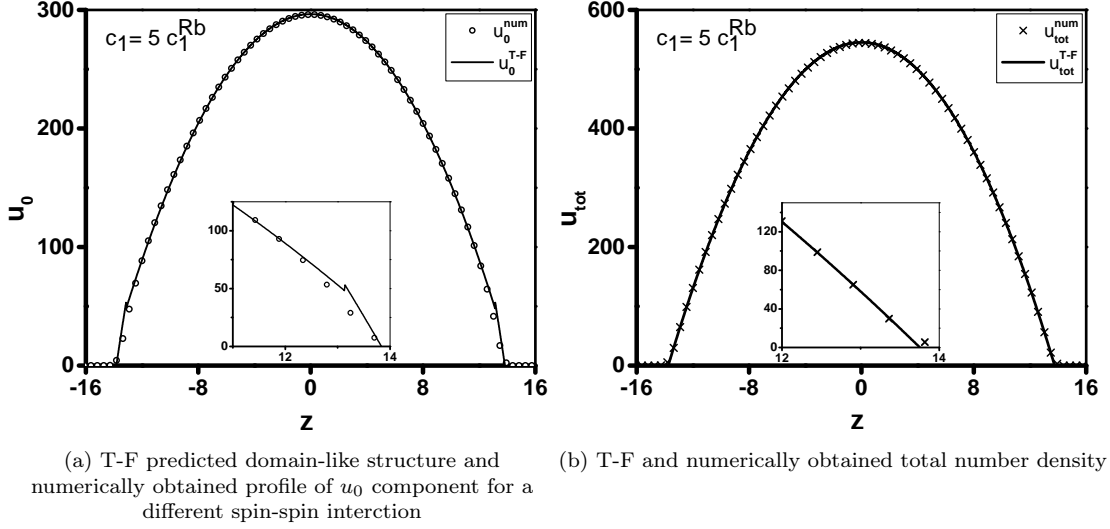


Figure 3. Subfig-(a): The T-F sub-component number density u_0 for PM state for the same the parameter values $p' = 0.01$ and $q' = 0.3$ and λ_0 but for a different spin-dependent interaction coefficient c_1 (see Eq.4) which is now 5 times of that of ^{87}Rb [63]. The PM-like followed by polar-like u_0 has a distinct discontinuity at $|\zeta_{\pm 1}^{TF}| = 13.13$ (see inset). Subfig-(b): The numerical total number density follows Eq. 20. (See inset) The analytical and the numerical total number density agree across $|\zeta_{\pm 1}^{TF}|$ but a visible deviation comes near the tail of the condensate where kinetic energy contribution is the most significant.

matching points can be found from the minimization of the total energy. Once the matching points are obtained we can write the analytical expressions for all the sub-component densities.

Following the numerical evidence that the total number density follows Eq.20 (see Fig.2), it is sensible to apply the multi-modal VM for total number density and the $u_{\pm 1}$. The u_0 expression can be later found out by subtracting the sum of variational profiles of $n_{\pm 1}$ from the total number density profile, i.e., $u_0^{VM} = u_{tot}^{VM} - u_1^{VM} - u_{-1}^{VM}$. So for simplicity, instead of the u_0 component, we will focus on total number density which will also provide a matching point ζ_{tot}^{mat} . Note that, for the PM state, the spatial mode for the u_1 and u_{-1} are equivalent, so the matching point for those two sub-components will be the same i.e., $\zeta_1^{mat} = \zeta_{-1}^{mat}$. Thus, the minimization of the total energy in the two-dimensional parameter space of ζ_1^{mat} and ζ_{tot}^{mat} will determine the energy itself as well as approximate values of these parameters.

From the minimization of total energy for this particular case, we find that the matching points are, $\zeta_1^{mat} = \zeta_{-1}^{mat} = 7.98$ and $\zeta_{tot}^{mat} = 13.41$ and the corresponding value of the parameter, $\mu' = 95.46$. Thus, the analytical number densities can be written as,

$$u_1^{var} = \begin{cases} 1.5173(53.0977 - 0.5\zeta^2), & \text{if } |\zeta| \leq 7.978 \\ 1.5173(9308.6737 - 2838.3002|\zeta| \\ + 229.4058\zeta^2)\exp(-0.0642\zeta^2), & \text{otherwise,} \end{cases} \quad (23)$$

$$u_{-1}^{var} = \begin{cases} 1.3278(53.0977 - 0.5\zeta^2), & \text{if } |\zeta| \leq 7.978 \\ 1.3278(9308.6737 - 2838.3002|\zeta| \\ + 229.4058\zeta^2)\exp(-0.0642\zeta^2), & \text{otherwise,} \end{cases} \quad (24)$$

$$u_{tot}^{var} = \begin{cases} 5.6839(95.4569 - 0.5\zeta^2), & \text{if } |\zeta| \leq 13.412 \\ 5.6839(8.895 \times 10^{24} - 1.3539 \times 10^{24}|\zeta| \\ + 5.1533 \times 10^{22}\zeta^2)\exp(-0.2692\zeta^2), & \text{otherwise,} \end{cases} \quad (25)$$

where the numbers are rounded up to four decimal places as it may cause a large rounding error in the density expressions. Note that, in Eq.25 the coefficients of the total number density might look very large, but for $|\zeta| \geq 13.412$ where the expression is valid, the contribution from the exponential part is so small that the combined contribution asymptotically goes to zero at large distances and matches quite accurately with the numerical profile (see the inset of Fig.4(b))

We have made a case study of the PM state which is a multi-component stationary state that becomes the ground state for a range of linear and quadratic Zeeman strengths. For the purpose of comparison with numerical simulation, we have chosen 1-D harmonic trapping and particular values of p , q , and the number of condensate particles N .

Note that the VM is an approximation scheme that

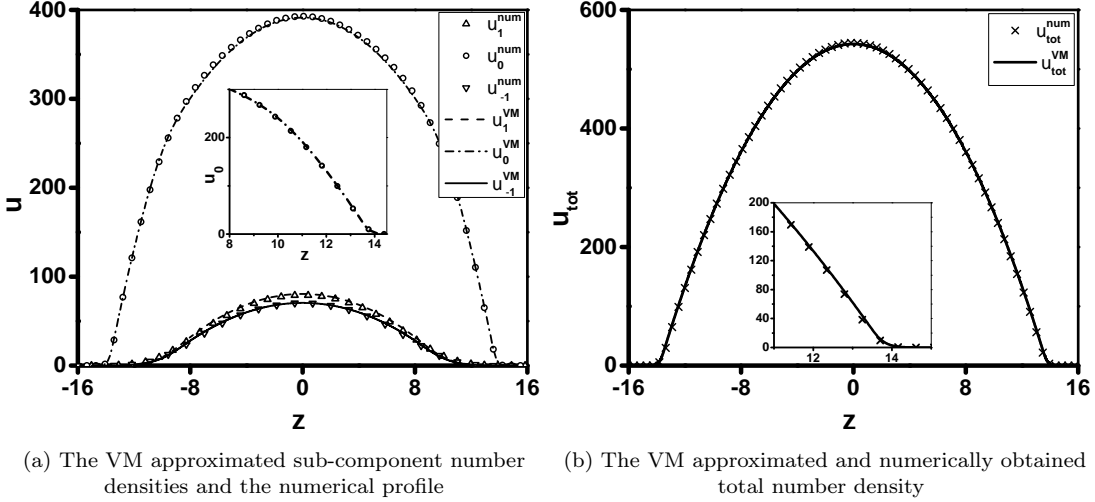


Figure 4. Subfig-(a): The sub-component number density of the PM state obtained via the numerical and variational methods are plotted against the distance from the trap center ζ . The VM produces a very good analytical profile that describes the numerical data quite well even in the tail part of the condensate. The VM rules out any domain-like possibility and analytically estimates the u_0 component (shown in the dash-dot line) that is quite accurate in comparison to the numerical (circles) profile (see inset). Subfig-(b): The variationally obtained total number density provides an excellent analytical profile to match the numerical result near the core of the trap as well as in the low-density region, where it gives an analytic estimate of the condensate density which asymptotically goes to zero with the increase of the distance ζ .

works really well in estimating the sub-component number densities (also the mean fields) which produces a very good estimation of the vector order parameter of the spin-1 system. Like other approximate methods, it has some limitations as well. For example, at a large distance from the center of the trap (very large ζ), where the total density u_{tot}^{VM} and $u_{\pm 1}^{VM}$ are very close to zero and can be considered negligible, we find that the total density is slightly lesser than the combined contribution of the ± 1 sub-components hence, making u_0^{VM} slightly negative which is not physical. For this reason, we have taken the contribution up to a large ζ after which we assume that u_0 goes to zero. Thus the kinetic energy contribution is included and considered up to a large distance without discontinuity.

In the next section, we will do a brief case study on the anti-ferromagnetic state which is the other possible multi-component stationary state that becomes the ground state for ^{23}Na .

C. Anti-ferromagnetic state

For the ^{23}Na -condensate which has an anti-ferromagnetic type of spin-spin interaction ($c_1 > 0$), we set the same trapping frequencies corresponding to 1-D confinement as mentioned earlier for the ferromagnetic type condensate. The oscillator length in elongated direction $l_x = 2.97 \mu\text{m}$ and in the transverse direction $l_{yz} = 0.59 \mu\text{m}$. Note that, although we consider the same trapping geometry, the oscillator length scale

for ^{23}Na and ^{87}Rb condensates are different due to the different masses of the species. The non-dimensional spin-independent and spin-spin interaction parameters are $\lambda_0 = 46.16 \times 10^{-3}$ and $\lambda_1 = 7.43 \times 10^{-4}$ corresponding to the values given in [63]. For a range of linear and quadratic Zeeman terms, the anti-ferromagnetic (AF) state is found to be favorable to be the ground state. For the purpose of numerical study, we focus on the case these terms are fixed at $p' = 0.2$ and $q' = -0.5$.

As long as the u_1 and u_{-1} sub-components are non-zero, the T-F approximation gives an estimation of the total as well as sub-component number densities (see Table 1),

$$u_1^{TF} = \frac{\mu' - q' - \zeta^2/2}{2\lambda_0} + \frac{p'}{2\lambda_1}, \quad (26)$$

$$u_{-1}^{TF} = \frac{\mu' - q' - \zeta^2/2}{2\lambda_0} - \frac{p'}{2\lambda_1}. \quad (27)$$

As the value of p' is chosen as positive (and λ_1 is positive as well) the u_{-1} component goes to zero much faster than the other one. So beyond the T-F radius of the u_{-1} component the AF state ceases to exist. As the u_1 component is still non-zero, so according to T-F, the situation is domain-like with AF state at the center of the trap followed by the ferromagnetic state outside (for $|\zeta| > \zeta_{-1}^{TF}$).

Just like the PM state that we have seen earlier, the numerical simulation does not vindicate the domain-like prediction. Rather the AF state is found to be present for

all values of ζ . The VM can be applied to get an analytical explanation of the situation for this multi-component state.

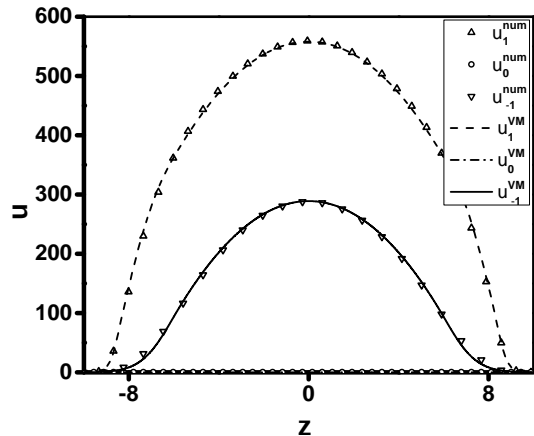


Figure 5. Sub-component density expressions obtained via VM are compared with the numerical profile for the anti-ferromagnetic state with the Zeeman terms fixed at $p' = 0.2$ and $q' = -0.5$. The density expressions obtained from VM for $u_{\pm 1}$ are shown in dashed and solid lines respectively, which agrees quite well with the numerical results both in high- and low-density regions.

Following the same procedure as described for PM state one can apply the VM for the total density and the sub-component density u_{-1} . The u_0 component is empty and there will be two matching points ζ_{tot}^{mat} and ζ_{-1}^{mat} that are to be found out from the minimization of the total energy. For the previously mentioned p' and q' values, we get these two matching points to be, $\zeta_{tot}^{mat} = 8.36$ and $\zeta_{-1}^{mat} = 5.79$. These also produce the analytical formulae of the total density and the u_{-1} components. The density expression for u_1 component can be obtained by subtracting the other sub-component density from the total density.

The VM shows that the domain-like situation that the T-F predicts is incorrect and justifies the fact that the kinetic energy terms cannot be neglected at least near the T-F radius for the sub-component which is of smaller density, in this case, the u_{-1} component. The VM also produces a low-density expression of the u_{-1} component which has a small but non-zero presence beyond u_{-1}^{TF} . Thus, it is only the AF state that is present for all regions of space. Moreover, the analytic number density expressions obtained from VM corresponding to each sub-component are in fair agreement with the numerically obtained profiles (see Fig.5).

IV. DISCUSSION

In this article, we have discussed the inaccuracy of the T-F as the most widely used analytical method to describe the multi-component states of a trapped spin-1

BEC in presence of the magnetic field. The T-F approximation leads to a wrong conclusion about the existence of the domain-like structure while explaining the ground state structure involving multi-component stationary states even in the so-called "T-F regime", where the density of the condensate is high enough to neglect the kinetic energy contribution in comparison to the interaction terms. We have extended the multi-modal variational method introduced in [1] to the presence of the magnetic field. We have shown that the variational method successfully describes the density distribution of the multi-component states which is also backed by numerical simulation. The VM properly captures the multi-component states because it can estimate the tail part of the components with smaller densities where T-F cuts it off. These tail parts of the densities reside in a region where the kinetic energy contributions are most significant and cannot be neglected even if it is small.

For this study, we focus on multi-component states with fixed values of linear and quadratic Zeeman terms. We also considered a fixed value of the total number of condensate particles, N . However, this procedure is applicable for different values of these parameters. The VM can be easily implemented for 3-D harmonic trapping to get the details of all the stationary states including all the multi-component states. Whereas, doing numerical simulation for a 3-D system is well-known to be computationally expensive. Note that for single-component stationary states (like ferromagnetic and polar states), the T-F gives fairly accurate results in comparison to the numerical simulation in the T-F regime. Still, the variational method finds its importance which incorporates the kinetic energy contribution and predicts the condensate profile even in the low-density region with fair accuracy. Specifically for condensates with a smaller number of particles where the kinetic energy term is comparable to the interaction energy, T-F is in general, not applicable and the VM is indispensable as an analytical method [1]. This is true even for non-zero contributions of p and q .

The VM is obviously an approximation scheme but it provides a good analytical profile of the condensate. Note that, many studies require a numerically exact ground state profile of a spin-1 condensate under trapping in presence of a magnetic field. This analytical method provided here would also find its relevance in such cases if one uses the VM approximated density profile as an initial condition for quick convergence to the numerical profile.

The ground state structure and the phase diagram of a trapped spin-1 condensate in the p, q parameter space are of fundamental relevance. The total energy corresponding to different stationary states can be compared which reveals the stationary state that becomes the ground state for different values of p and q . Thus, an accurate analytical description of all the stationary states, specifically the multi-component states is required. Therefore, the method involving the variational procedure shown

here is of fundamental importance and becomes a prerequisite to such a tedious study.

V. ACKNOWLEDGEMENT

PKK would like to thank the Council of Scientific and Industrial Research (CSIR), India for providing funding during this research. The support and the resources pro-

vided by PARAM Brahma Facility under the National Supercomputing Mission, Government of India at the Indian Institute of Science Education and Research; Pune are gratefully acknowledged.

Data availability statement: The datasets generated and analyzed during the current study are available from the corresponding author at a reasonable request.

-
- [1] Kanjilal, Projjwal Kanti and Bhattacharyay, A., *Eur. Phys. J. Plus* **137**, 547 (2022).
 - [2] K. B. Davis, M. O. Mewes, M. R. Andrews, N. J. van Druten, D. S. Durfee, D. M. Kurn, and W. Ketterle, *Phys. Rev. Lett.* **75**, 3969 (1995).
 - [3] M. H. Anderson, J. R. Ensher, M. R. Matthews, C. E. Wieman, and E. A. Cornell, *Science* **269**, 198 (1995).
 - [4] C. C. Bradley, C. A. Sackett, J. J. Tollett, and R. G. Hulet, *Phys. Rev. Lett.* **75**, 1687 (1995).
 - [5] S. Giorgini, L. P. Pitaevskii, and S. Stringari, *Phys. Rev. A* **54**, R4633 (1996).
 - [6] F. Dalfovo and S. Stringari, *Phys. Rev. A* **53**, 2477 (1996).
 - [7] S. Stringari, *Phys. Rev. Lett.* **77**, 2360 (1996).
 - [8] N. Dupont, G. Chatelain, L. Gabardos, M. Arnal, J. Billy, B. Peaudecerf, D. Sugny, and D. Guéry-Odelin, *PRX Quantum* **2**, 040303 (2021).
 - [9] R. Senaratne, S. V. Rajagopal, T. Shimasaki, P. E. Dotti, K. M. Fujiwara, K. Singh, Z. A. Geiger, and D. M. Weld, *Nat Commun* **9**, 2065 (2018).
 - [10] Y. Yamamoto and Y. Takahashi, “Bose-einstein condensation: A platform for quantum simulation experiments,” in *Principles and Methods of Quantum Information Technologies*, edited by Y. Yamamoto and K. Semba (Springer Japan, Tokyo, 2016) pp. 265–307.
 - [11] T. Bravo, C. Sabín, and I. Fuentes, *EPJ Quantum Technology* **2**, 3 (2015).
 - [12] J. I. Cirac and P. Zoller, *Nature Physics* **8**, 264 (2012).
 - [13] I. M. Georgescu, S. Ashhab, and F. Nori, *Rev. Mod. Phys.* **86**, 153 (2014).
 - [14] D. Becker, M. D. Lachmann, S. T. Seidel, H. Ahlers, A. N. Dinkelaker, J. Grosse, O. Hellmig, H. Müntinga, V. Schkolnik, T. Wendrich, A. Wenzlawski, B. Weps, R. Corgier, T. Franz, N. Gaaloul, W. Herr, D. Lüdtke, M. Popp, S. Amri, H. Duncker, M. Erbe, A. Kohfeldt, A. Kubelka-Lange, C. Braxmaier, E. Charron, W. Ertmer, M. Krutzik, C. Lämmerzahl, A. Peters, W. P. Schleich, K. Sengstock, R. Walser, A. Wicht, P. Windpassinger, and E. M. Rasel, *Nature* **562**, 391 (2018).
 - [15] S. S. Zigei, S. P. Nolan, J. D. Close, and S. A. Haine, *Phys. Rev. Lett.* **125**, 100402 (2020).
 - [16] S. Gupta, K. Dieckmann, Z. Hadzibabic, and D. E. Pritchard, *Phys. Rev. Lett.* **89**, 140401 (2002).
 - [17] A. O. Jamison, J. N. Kutz, and S. Gupta, *Phys. Rev. A* **84**, 043643 (2011).
 - [18] D. Hanneke, S. Fogwell, and G. Gabrielse, *Phys. Rev. Lett.* **100**, 120801 (2008).
 - [19] P. Dutta, S. S. Maurya, K. Patel, K. Biswas, J. Man-gaonkar, S. Sarkar, and U. D. Rapol, *Journal of the Indian Institute of Science* (2022), 10.1007/s41745-022-00335-8.
 - [20] J. R. Ensher, D. S. Jin, M. R. Matthews, C. E. Wieman, and E. A. Cornell, *Phys. Rev. Lett.* **77**, 4984 (1996).
 - [21] J. R. Ensher, D. S. Jin, M. R. Matthews, C. E. Wieman, and E. A. Cornell, *Phys. Rev. Lett.* **77**, 4984 (1996).
 - [22] W. Ketterle, M. R. Andrews, K. B. Davis, D. S. Durfee, D. M. Kurn, M. O. Mewes, and N. J. van Druten, *Physica Scripta* **1996**, 31 (1996).
 - [23] D. M. Stamper-Kurn, M. R. Andrews, A. P. Chikkatur, S. Inouye, H.-J. Miesner, J. Stenger, and W. Ketterle, *Phys. Rev. Lett.* **80**, 2027 (1998).
 - [24] M.-S. Chang, C. D. Hamley, M. D. Barrett, J. A. Sauer, K. M. Fortier, W. Zhang, L. You, and M. S. Chapman, *Phys. Rev. Lett.* **92**, 140403 (2004).
 - [25] D. M. Stamper-Kurn and W. Ketterle, in *Les Houches - Ecole d’Ete de Physique Theorique* (Springer Berlin Heidelberg) pp. 139–217.
 - [26] Y. Kawaguchi, H. Saito, and M. Ueda, *Phys. Rev. Lett.* **97**, 130404 (2006).
 - [27] A. E. Leanhardt, Y. Shin, D. Kielpinski, D. E. Pritchard, and W. Ketterle, *Phys. Rev. Lett.* **90**, 140403 (2003).
 - [28] E. Timmermans, *Phys. Rev. Lett.* **81**, 5718 (1998).
 - [29] T. Świsłocki and M. Matuszewski, *Phys. Rev. A* **85**, 023601 (2012).
 - [30] K.-T. Xi, J. Li, and D.-N. Shi, *Phys. Rev. A* **84**, 013619 (2011).
 - [31] S. Bandyopadhyay, A. Roy, and D. Angom, *Phys. Rev. A* **96**, 043603 (2017).
 - [32] T. Isoshima, K. Machida, and T. Ohmi, *Phys. Rev. A* **60**, 4857 (1999).
 - [33] M. Matuszewski, T. J. Alexander, and Y. S. Kivshar, *Phys. Rev. A* **78**, 023632 (2008).
 - [34] M. Matuszewski, T. J. Alexander, and Y. S. Kivshar, *Phys. Rev. A* **80**, 023602 (2009).
 - [35] T.-L. Ho and V. B. Shenoy, *Phys. Rev. Lett.* **77**, 3276 (1996).
 - [36] S. Bhuvaneswari, K. Nithyanandan, and P. Muruganandam, *Journal of Physics Communications* **2**, 025008 (2018).
 - [37] L. Wen, W. M. Liu, Y. Cai, J. M. Zhang, and J. Hu, *Phys. Rev. A* **85**, 043602 (2012).
 - [38] Z. Liu, *Journal of Mathematical Physics* **50**, 102104 (2009), <https://doi.org/10.1063/1.3243875>.
 - [39] L. Zhu and J. Li, *Modern Physics Letters B* **31**, 1750215 (2017), <https://doi.org/10.1142/S0217984917502153>.
 - [40] S. Tojo, Y. Taguchi, Y. Masuyama, T. Hayashi, H. Saito, and T. Hirano, *Phys. Rev. A* **82**, 033609 (2010).
 - [41] J. Li, Y.-M. Yu, K.-J. Jiang, and W.-M. Liu, arXiv

- preprint arXiv:1802.00138 (2018).
- [42] K. L. Lee, N. B. Jørgensen, I.-K. Liu, L. Wacker, J. J. Arlt, and N. P. Proukakis, *Phys. Rev. A* **94**, 013602 (2016).
 - [43] J. Sabbatini, W. H. Zurek, and M. J. Davis, *Phys. Rev. Lett.* **107**, 230402 (2011).
 - [44] S. Gautam and S. K. Adhikari, *Phys. Rev. A* **90**, 043619 (2014).
 - [45] S. Gautam and D. Angom, *Journal of Physics B: Atomic, Molecular and Optical Physics* **44**, 025302 (2011).
 - [46] H. Saito and M. Ueda, *Phys. Rev. A* **72**, 023610 (2005).
 - [47] P. K. Kanjilal and A. Bhattacharyay, *Physica Scripta* **95**, 045702 (2020); *Physica Scripta* **97**, 129501 (2022).
 - [48] M. Ueda, *Reports on Progress in Physics* **77**, 122401 (2014).
 - [49] H. E. Nistazakis, D. J. Frantzeskakis, P. G. Kevrekidis, B. A. Malomed, and R. Carretero-González, *Phys. Rev. A* **77**, 033612 (2008).
 - [50] T. M. Bersano, V. Gokhroo, M. A. Khamsehchi, J. D'Ambroise, D. J. Frantzeskakis, P. Engels, and P. G. Kevrekidis, *Phys. Rev. Lett.* **120**, 063202 (2018).
 - [51] G. C. Katsimiga, S. I. Mistakidis, P. Schmelcher, and P. G. Kevrekidis, *New Journal of Physics* **23**, 013015 (2021).
 - [52] G. Hegde, S. M. Jose, and R. Nath, *Phys. Rev. A* **106**, 043307 (2022).
 - [53] S. I. Mistakidis, A. G. Volosniev, R. E. Barfknecht, T. Fogarty, T. Busch, A. Foerster, P. Schmelcher, and N. T. Zinner, “Cold atoms in low dimensions – a laboratory for quantum dynamics,” (2022).
 - [54] T.-L. Ho, *Phys. Rev. Lett.* **81**, 742 (1998).
 - [55] S. Yi, O. E. Müstecaplıoğlu, C. P. Sun, and L. You, *Phys. Rev. A* **66**, 011601 (2002).
 - [56] W. Zhang, S. Yi, and L. You, *New Journal of Physics* **5**, 77 (2003).
 - [57] S. Gautam and S. K. Adhikari, *Phys. Rev. A* **92**, 023616 (2015).
 - [58] N. T. Phuc, Y. Kawaguchi, and M. Ueda, *Phys. Rev. A* **84**, 043645 (2011).
 - [59] Y. Kawaguchi, N. T. Phuc, and P. B. Blakie, *Phys. Rev. A* **85**, 053611 (2012).
 - [60] E. Serrano-Ensajstiga and F. Mireles, “Spinor bose-einstein condensates: self-consistent symmetries and characterization,” (2022).
 - [61] K. M. Mittal, S. I. Mistakidis, P. G. Kevrekidis, and P. Schmelcher, *Phys. Rev. A* **102**, 013302 (2020).
 - [62] J. Stenger, S. Inouye, D. Stamper-Kurn, H.-J. Miesner, A. Chikkatur, and W. Ketterle, *Nature* **396**, 345 (1998).
 - [63] Y. Kawaguchi and M. Ueda, *Physics Reports* **520**, 253 (2012), spinor Bose–Einstein condensates.
 - [64] T. Ohmi and K. Machida, *Journal of the Physical Society of Japan* **67**, 1822 (1998).
 - [65] P. Kaur, A. Roy, and S. Gautam, *Computer Physics Communications* **259**, 107671 (2021).
 - [66] D. J. Papoular, G. V. Shlyapnikov, and J. Dalibard, *Phys. Rev. A* **81**, 041603 (2010).

Appendix A: Variational Method

To work with the non-zero contribution of p and q , we extend the variational method introduced in the article [1]. First, we will present the general method in a brief

manner and then we will implement that for the PM state and the AF state which are the multi-component states of interest to this article.

To implement the variational method, in presence of quasi-one-dimensional harmonic trapping, one needs to solve the GP equations Eq.13-14 by getting rid of the kinetic energy terms which will yield the sub-component densities in the high-density region near the center of the trap, where the kinetic energy can be neglected in comparison to the interaction terms. The sub-component densities will get a functional form specific to different stationary states. Next, we assume that near the low-density region where the kinetic energy is of relevance and the interaction terms are very small, the mean fields can be described in terms of the first few oscillator states. Thus the density distributions can be written as,

$$u_{\pm 1,0}^{in} = g_{\pm 1,0}(\mu', \zeta), \quad \text{for } |\zeta| \leq \zeta_{\pm 1,0}^{mat} \quad (\text{A1})$$

$$u_{\pm 1,0}^{out} = (a_{\pm 1,0} + c_{\pm 1,0}|\zeta| + d_{\pm 1,0}\zeta^2) \exp\left(-\frac{\zeta^2}{b_{\pm 1,0}}\right) \quad \text{for } |\zeta| \geq \zeta_{\pm 1,0}^{mat}, \quad (\text{A2})$$

where, $u_{\pm 1,0}^{in(out)}$ is the sub-component densities in the high-(low-)density region. Now we impose the condition that for each sub-component the low-density $\sqrt{u_{\pm 1,0}^{out}}$ and the high-density $\sqrt{u_{\pm 1,0}^{in}}$ expressions match at a point ζ^{mat} . Not only do they match but their first three derivatives also match. These four constraints provide the four unknowns a , b , c , and d for each sub-components in terms of the matching points and the parameter μ' . Note that, imposing the matching condition up to three derivatives also gives a smooth profile of the corresponding kinetic energy.

Once all the coefficients in Eq.A2 are known, the sub-component density profile only depends on the parameter μ' and the matching points. The parameter μ' can be obtained as a function of the matching points from,

$$\sum_{m=-1}^1 \left[\int_0^{\zeta_m^{mat}} u_m^{in}(\mu', \zeta) d\zeta + \int_{\zeta_m^{mat}}^{\infty} u_m^{out}(\mu', \zeta, \zeta_m^{mat}) d\zeta \right] = N, \quad (\text{A3})$$

where N is the total number of condensate particles. Note that, one might expect that the right side should be $N/2$ as the integration is running in only one direction from the center of the trap, but it is N in the right side due to the Eq.11-12 which we used to write the GP equation in non-dimensional form. From this Eq.A3 the parameter μ' can be written as a function of the matching points for a particular N .

Thus the sub-component number densities and hence the total energy of a stationary state (Eq.10) also becomes the function of the matching points only. Now minimization of the total energy in the parameter space of the matching points one can get the matching points as well as the total energy itself.

1. Variational method for the PM state:

For the PM state, all the sub-components are populated followed by the phase matching condition, i.e., the relative phase being $\theta_r = 0$. One can solve the phase stationary equations (Eq.13-14) by ignoring the kinetic part to get the sub-component densities in the high-density region as,

$$u_m^{in} = k_m \left[\frac{\mu'_m - \zeta^2/2}{\lambda_0 + \lambda_1} \right], \quad (\text{A4})$$

where,

$$\begin{aligned} k_1 &= \frac{(p' + q')^2}{4q'^2} \\ k_0 &= \frac{q'^2 - p'^2}{2q'^2} \\ k_{-1} &= \frac{(p' - q')^2}{4q'^2} \end{aligned} \quad (\text{A5})$$

and,

$$\begin{aligned} \mu'_{\pm 1} &= \mu'_{eff} + (\lambda_0 + \lambda_1) \frac{q'^2 - p'^2}{2\lambda_1 q'}, \\ \mu'_0 &= \mu'_{eff} - (\lambda_0 + \lambda_1) \frac{q'^2 + p'^2}{2\lambda_1 q'}, \\ \mu'_{eff} &= \mu' + \frac{p'^2 - q'^2}{2q'}. \end{aligned} \quad (\text{A6})$$

Once, we write the sub-component densities in the high-density region in such a compact form like Eq.A4 one can apply the four matching conditions mentioned earlier-. This would allow us to get the four unknown coefficients in the low-density expression for each sub-component,

$$a_m = \frac{1}{-8\mu'_m + 4\zeta_m^2} \left(\mu'_m (-56\mu'_m + 70\zeta_m^2 + 4\kappa_m) - 3\zeta_m^2 (14\zeta_m^2 + \kappa_m - 6\mu'_m) \right) \exp\left(\frac{12\zeta_m^2}{\kappa_m}\right), \quad (\text{A7})$$

$$b_m = \frac{\kappa_m}{12}, \quad (\text{A8})$$

$$c_m = \frac{48\zeta_m^3 (-12\mu'_m + 6\zeta_m^2 + \kappa_m)}{\kappa_m^2} \exp\left(\frac{12\zeta_m^2}{\kappa_m}\right), \quad (\text{A9})$$

$$\begin{aligned} d_m &= \frac{1}{2\zeta_m^2 (-2\mu'_m + \zeta_m^2)} \left(-6(\mu'_m)^2 - \zeta_m^2 (\kappa_m + 13\zeta_m^2 - 6\mu'_m) \right. \\ &\quad \left. + \mu'_m (14\zeta_m^2 + \kappa_m - 6\mu'_m) \right) \exp\left(\frac{12\zeta_m^2}{\kappa_m}\right), \end{aligned} \quad (\text{A10})$$

where, ζ_m is an abbreviation for the matching point ζ_m^{mat} and,

$$\begin{aligned} \kappa_m &= 6\mu'_m - 9\zeta_m^2 \\ &\quad + \sqrt{36\mu_m^2 - 12\mu_m\zeta_m^2 + 33\zeta_m^4}, \end{aligned} \quad (\text{A11})$$

given one writes the sub-component densities in the low-density region as,

$$u_m^{out} = \frac{k_m}{\lambda_0 + \lambda_1} \left(a_m + c_m |\zeta| + d_m \zeta^2 \right) \exp\left(-\frac{\zeta^2}{b_m}\right). \quad (\text{A12})$$

Now applying Eq.A3 one can find the parameter μ' for different values of ζ_m . Note that, as $\mu'_1 = \mu'_{-1}$ (see Eq.A6) the matching points are the same for these two

components, i.e., $\zeta_1^{mat} = \zeta_{-1}^{mat}$. Thus, the total energy (Eq.10) for the PM state becomes only a function of the matching points.

Note that, from a physical perspective, the high-density expressions of u_0 and $u_{\pm 1}$ were found by getting rid of the kinetic terms in the Eq.13-14. So the high-density expressions given in Eq.A4 are true as long as all the sub-components are in the high-density region. If we focus on the case presented in the article, for $p' = 0.01$ and $q' = 0.3$, near T-F radius the $u_{\pm 1}$ sub-component does not follow the high-density expressions. As a result, one can neglect the derivative term in Eq.13 but cannot neglect the same in Eq.14. This precisely makes the multi-component stationary states beyond the reach of T-F approximation as long as the sub-components are multi-modal in nature.

Precisely because of the reason stated above one has to shift the focus toward the total density. So, instead of using the high-density expression u_0^{in} we will use the total density expression,

$$u_{tot}^{in} = k_{tot} \left[\frac{\mu'_{eff} - \zeta^2/2}{\lambda_0 + \lambda_1} \right], \quad (A13)$$

written in the same fashion as Eq.A4, where $k_{tot} = 1$ and the μ_{eff} can be found in Eq.A6. Now instead of putting $m = 0$, one can put $m = tot$ in Eq.A7-A10 which would provide the total density expression in the low-density region (putting $m = tot$ in Eq.A12). The u_0 component can be found by subtracting the other two component densities from the total density.

Now the total energy of the PM state only becomes a function of the two matching points, ζ_{tot}^{mat} and $\zeta_{\pm 1}^{mat}$. Minimizing the total energy with respect to these two parameter variations one can get the matching points and the total energy itself. And as the matching points are found, the analytical density expressions are also obtained.

2. Variational method for the AF state:

When the u_1 and the u_{-1} components are populated (even though they are unequally populated for non-zero values of p' (see Table 1)) the stationary state is referred to as the anti-ferromagnetic or in short, AF state. When

both the sub-components are in the high-density regions, one can write the densities by neglecting the derivative terms in the phase equations as,

$$u_{\pm 1}^{in} = k_{\pm 1} \left[\frac{\mu'_{\pm 1} - \zeta^2/2}{\lambda_0} \right], \quad (A14)$$

where, $k_{\pm 1} = 1/2$ and,

$$\mu'_{\pm 1} = \mu' - q' \pm \frac{\lambda_0}{\lambda_1} p'. \quad (A15)$$

The sub-component density u_0 is zero throughout.

Note that, the high energy expressions are valid as long as both the sub-component density is high enough so that the derivative terms can be safely ignored. But for $p' = 0.2$ and $q' = -0.5$ (the case we discussed), the u_{-1} component has a lesser T-F radius than the other component. As a result of it near the low-density region of the u_{-1} component the high-density expression of the u_1 component would be invalid, for the reasons stated earlier. So, we will take the total density and the u_{-1} component to implement the variational method.

In the high-density region, the total density can be written as,

$$u_{tot}^{in} = k_{tot} \left[\frac{\mu'_{tot} - \zeta^2/2}{\lambda_0} \right], \quad (A16)$$

where $k_{tot} = 1$. Now if one writes the low-density expressions as,

$$u_m^{out} = \frac{k_m}{\lambda_0} \left(a_m + c_m |\zeta| + d_m \zeta^2 \right) \exp \left(- \frac{\zeta^2}{b_m} \right) \quad (A17)$$

where the subscript can be $m = -1, tot$. Now the coefficients will have the same expressions as Eq.A7-A11.

Following the same method as explained earlier one can minimize the total energy corresponding to this stationary state in the parameter space of the matching points ζ_{tot} and ζ_{-1} which provides the analytical form of the full profile of the condensate in terms of the total density and the u_{-1} component. By subtracting the u_{-1} component from the total density profile one can get to the u_1 component.